Caroline André,[1,2] Omar Guzman-Quevedo,[1,2,3] Charlotte Rey,[4,5] Julie Rémus-Borel,[4,5] Samantha Clark,[1,2] Ashley Castellanos-Jankiewicz,[1,2] Elodie Ladeveze,[1,2] Thierry Leste-Lasserre,[1,2] Agnes Nadjar,[4,5] Djoher Nora Abrous,[1,2] Sophie Laye,[4,5] and Daniela Cota[1,2]

Inhibiting Microglia Expansion Prevents Diet-Induced Hypothalamic and Peripheral Inflammation

OBESITY STUDIES

Cell proliferation and neuroinflammation in the adult hypothalamus may contribute to the pathogenesis of obesity. We tested whether the intertwining of these two processes plays a role in the metabolic changes caused by 3 weeks of a high–saturated fat diet (HFD) consumption. Compared with chow-fed mice, HFD-fed mice had a rapid increase in body weight and fat mass and specifically showed an increased number of microglia in the arcuate nucleus (ARC) of the hypothalamus. Microglia expansion required the adequate presence of fats and carbohydrates in the diet because feeding mice a very high-fat, very low-carbohydrate diet did not affect cell proliferation. Blocking HFD-induced cell proliferation by central delivery of the antimitotic drug arabinofuranosyl cytidine (AraC) blunted food intake, body weight gain, and adiposity. AraC treatment completely prevented the increase in number of activated microglia in the ARC, the expression of the proinflammatory cytokine tumor necrosis factor-α in microglia, and the recruitment of the nuclear factor-κB pathway while restoring hypothalamic leptin sensitivity. Central blockade of cell proliferation also normalized circulating levels of the cytokines leptin and interleukin 1β and decreased peritoneal proinflammatory CD86 immunoreactive macrophage number. These findings suggest that inhibition of diet-dependent microglia expansion hinders body weight gain while preventing central and peripheral inflammatory responses due to caloric overload.

Consumption of a high saturated fat diet favors metabolic disorders by causing inflammation in peripheral organs (1–3). High-fat diet (HFD)–induced peripheral inflammation is associated with inflammation in brain areas such as the hippocampus and the hypothalamus (4–8). In particular, inflammation in the mediobasal hypothalamus, including the arcuate nucleus (ARC), happens rapidly, before obesity is established (9). Within the ARC, agouti-related protein (AgRP)– and proopiomelanocortin (POMC)–producing neurons sense and integrate nutrient and hormonal signals to guarantee energy homeostasis (10,11). Hypothalamic inflammation causes changes in ARC neurons and, in turn, is responsible for diet-induced obesity (9,12,13) and insulin resistance in peripheral organs (14). Studies have shown that activation of the inflammatory nuclear factor-κB (NF-κB) pathway and recruitment of proinflammatory microglia in the hypothalamus lead to obesity (9,12,15,16). HFD intake can also induce cell proliferation and eventually neurogenesis in the adult hypothalamus, which in turn modifies the neural circuitry regulating energy balance (17).

We hypothesized that cell proliferation plays a key role in the central inflammatory response to HFD and investigated whether modulation of cell proliferation affects adaptive behavioral and metabolic changes related to caloric overload. Thus, mice were fed a chow diet or switched to a diet high in saturated fat. To control for the impact of fat and carbohydrate content on cell proliferation, chow-fed

[1]INSERM, Neurocentre Magendie, Physiopathologie de la Plasticité Neuronale, U1215, Bordeaux, France

[2]University of Bordeaux, Neurocentre Magendie, Physiopathologie de la Plasticité Neuronale, U1215, Bordeaux, France

[3]Facultad de Químico-Farmacobiología, Universidad Michoacána de San Nicolás de Hidalgo, Morelia, Michoacán, Mexico

[4]INRA, Nutrition et Neurobiologie Intégrée, UMR 1286, Bordeaux, France

[5]University of Bordeaux, Nutrition et Neurobiologie Intégrée, UMR 1286, Bordeaux, France

Corresponding authors: Daniela Cota, daniela.cota@inserm.fr, and Djoher Nora Abrous, nora.abrous@inserm.fr.

mice also were switched to a very high-fat, very low-carbohydrate diet (VHFD). Simultaneously, we blocked cell proliferation by centrally delivering the antimitotic drug arabinofuranosyl cytidine (AraC) and evaluated changes in energy balance, microglia activity, and inflammation. These studies revealed that HFD feeding specifically induces hypothalamic microglia expansion and that inhibition of HFD-induced cell genesis blunts food intake and adiposity while preventing hypothalamic and peripheral inflammation.

RESEARCH DESIGN AND METHODS

Animal Experimental Procedure
Experiments were performed according to European Union recommendations (2010/63/EU) after approval from the French Ministry of Agriculture and Fisheries (authorization number 3309004) and the ethics committee of the University of Bordeaux. Seven-week-old male C57BL/6J mice (Janvier Labs, Le Genest-Saint-Isles, France) were individually housed at 22°C with a 12-h light/dark cycle (lights off at 1:00 P.M.). Animals had free access to water and chow (Standard Rodent Diet A03; SAFE, Augy, France) unless stated otherwise (Table 1). Mice were acclimated for 1 week before the start of the study. One week after intracerebroventricular surgery, mice were either maintained on chow or switched to an HFD (D12492; Research Diets, New Brunswick, NJ). Mice were fed the HFD for up to 3 weeks (Supplementary Fig. 1A). In related studies, mice were fed chow or switched to a VHFD (D11111601; Research Diets) for 3 weeks. The VHFD was chosen so that the number of calories from saturated fat was similar to that of the HFD but with limited carbohydrates content, the major source of calories in chow.

Food intake and body weight were recorded daily. Feed efficiency was calculated as (body weight gained/caloric intake) $\times$ 100. At the end of the study, mice were either anesthetized and perfused for neuroanatomical analysis or killed by cervical dislocation and tissues and blood collected for molecular and biochemical analysis. The number of animals is detailed in the figure legends.

Intracerebroventricular Surgery
Eight-week-old mice were anesthetized with ketamine (100 mg/kg) and xylazine (10 mg/kg) and then implanted with a cannula into the lateral ventricle (anteroposterior −0.3 mm from bregma; lateral −1 mm to bregma; dorsoventral −2.5 mm below skull) by using a stereotaxic apparatus (David Kopf Instruments). The cannula was connected to an Alzet osmotic minipump (flow rate 0.11 μL/h for 4 weeks (model 1004; Alzet Charles River) through 120-mm vinyl tubing (inner diameter 0.69 mm) filled with artificial CSF (aCSF) (Tocris Bioscience). The minipumps were filled with aCSF containing 4.5 μg/μL BrdU (Sigma) with or without AraC 15 μg/μL (Sigma) and then primed overnight at 37°C in 0.9% saline.

Body Composition Analysis
Analysis was performed as previously described (18).

Western Blot Analysis
Proteins from hypothalami were extracted and quantified and Western blots carried out as previously described (19). Nitrocellulose membranes were incubated overnight at 4°C with rabbit anti–phospho-STAT3 (p-STAT3) (Tyr705, 1/4,000; Cell Signaling) or rabbit anti-inhibitor of κBα (IκBα) (1/1,000; Cell Signaling). After washing, membranes were incubated with a horseradish peroxidase–conjugated secondary antibody (goat anti-rabbit 1/2,000; Cell Signaling). Immunoreactive (IR) bands were revealed by using enhanced chemiluminescence (ECL Plus; PerkinElmer) and then exposed to radiographic films (Amersham Hyperfilm ECL; GE Healthcare Life Sciences). Membranes were stripped with 2-mercaptoethanol and then reblotted with rabbit anti-STAT3 (1/4,000; Cell Signaling). Blot quantification was performed with ImageJ software (National Institutes of Health, Bethesda, MD).

Hormone, Glucose, and Cytokine Measurements in Plasma
Plasma leptin and insulin were measured using ELISA kits from Abcam (Paris, France) and Mercodia (Uppsala, Sweden), respectively. Plasma glucose was measured with a glucose assay colorimetric kit (Abcam). Measurements were performed according to manufacturer instructions. HOMA of insulin resistance index was calculated as follows: (glucose mmol/L $\times$ insulin mU/L)/22.5.

Multiplex assays were performed according to manufacturer instructions (Bio-Rad) to quantify levels of plasma interleukin 1β (IL-1β) and tumor necrosis factor-α (TNF-α) (Milliplex MAP Mouse Cytokine/Chemokine Magnetic Bead Panel; Merck Millipore, Guyancourt,

Table 1—Characteristics of the diets used in the study

Type of diet	Caloric content (kcal/g)	Calories from macronutrients (%)		
		Fat	Carbohydrate	Protein
Chow (A03; SAFE)	3.2	14	61	25
HFD (D12492; Research Diets)	5.24	60[a]	20	20
VHFD (D11111601; Research Diets)	6.1	80[b]	5	16

[a]40% from saturated fatty acids. [b]50% from saturated fatty acids.

France) (5,20). Data were obtained by a Bio-Plex 200 system and analyzed with Bio-Plex Manager software (Bio-Rad).

Quantitative Real-Time PCR
Hypothalami were homogenized and quantitative real-time PCR reactions and analyses were performed as previously described (18). Reference genes were Nono and Sdha. Primer sequences are listed in Supplementary Table 1.

Isolation of Peritoneal Macrophages
Resident peritoneal macrophages were harvested by washing the peritoneal cavity with 10 mL of 1× PBS. Cells were centrifuged at 600g, and the cell pellet was suspended in PBS/BSA 0.1% for flow cytometry analysis.

Flow Cytometry
Cells were washed and incubated for 45 min with the following antibodies: anti-CD11b-APC, anti-CD45-PerCP Cy5.5, and anti-CD86-FITC (eBioscience) and anti-CD36-PE (BioLegend, Saint-Quentin-en-Yvelines, France). Cells were washed and suspended in PBS/BSA 0.1% for analysis. Nonspecific, isotype-matched antibodies were used to assess nonspecific binding. A BD Biosciences LSRFortessa multicolor flow cytometer was used to determine antigen expression. For each sample and isotype-matched conjugate, 10,000 events were recorded. Data were analyzed with FlowJo software, and gating for each antibody was determined on the basis of nonspecific binding of appropriate negative isotype-stained control.

Tissue Processing and Immunohistochemistry
Animals were anesthetized with 0.1 mL pentobarbital i.p. and perfused transcardially with cold 0.1 mol/L PBS, pH 7.4, followed by 4% buffered paraformaldehyde. Brains were collected, postfixed at 4°C overnight, and transferred into 30% sucrose solution at 4°C. Thirty-micrometer-thick free-floating coronal sections were cut with a cryostat (Leica) and stored in cryoprotectant medium (30% ethylene glycol, 30% glycerol in Krebs PBS) at −20°C until further processing. Antibodies used are listed in Supplementary Table 2.

Single immunolabelings were performed using similar procedures. Sections were incubated in 3% H_2O_2 in 1× PBS before blocking in 5% normal goat serum (Sigma) and 0.3% Triton X-100 in PBS for 1 h. Sections were incubated overnight with primary antibody at 4°C in blocking buffer. After washes, sections were incubated with secondary antibody in 1% normal goat serum-PBS for 2 h followed by 1-h incubation in a peroxidase-conjugated avidin/biotin complex solution (VECTASTAIN Elite ABC System; Vector Laboratories), and staining was visualized using a DAB Peroxidase (HRP) Substrate Kit (Vector Laboratories). Sections were washed in PBS and coverslipped. For BrdU immunostaining, sections were first incubated in a 3% H_2O_2 solution and then washed before treatment with 2 N HCl for 30 min at 37°C. Sections were then processed as described above. For phenotyping BrdU-labeled cells, a two-step procedure was performed. Sections were first

processed for ionized calcium-binding adapter molecule 1 (Iba1), glial fibrillary acidic protein (GFAP), and neuronal nuclei (NeuN) staining and then for BrdU. Sections were finally washed and coverslipped with mounting medium (ProLong Gold; Thermo Fisher Scientific).

Quantitative Analysis
For single 3,3′-diaminobenzidine immunodetection, digital images were captured by using a Leica DM5000 microscope. The numerical density of X-IR cells (N_v) or the total number of cells was estimated from counts made by systematic random sampling of every 10th section by a blind observer who used a semiautomatic neuron-tracing system (Neurolucida; MBF Bioscience).

The numerical density of Iba1-IR cells or BrdU-IR cells (number cells/mm^3) in the left- and right-side hypothalami was determined for at least three sections per brain containing the nucleus of interest. The number of cells was divided by the sectional volume of the area containing the ARC (from bregma −1.22 to bregma −2.70 mm), the paraventricular nucleus (PVN) (from bregma −0.34 to bregma −1.10 mm), or the ventromedial nucleus (from bregma −1.06 to bregma −2.00 mm). The same area was used for the same region investigated among the experimental groups.

The numerical density of Iba1-IR cells (number cells/mm^3) in the hippocampus was evaluated for at least five sections by using 50 × 50 × 10-μm frames at evenly spaced x-y intervals of 300 × 300 μm. N_v was calculated based on Eq. 1:

$$N_v = \frac{\Sigma Q^-}{h \times a(fra) \times \Sigma P} \qquad (Eq.\ 1)$$

where Q^- is the sum of cells, P is the number of frames, h is the dissector height, and a(fra) is the area of the counting frame. Cells in sharp focus in the uppermost focal plane were disregarded (optical dissector principle).

The total number of BrdU-IR cells in the dentate gyrus was quantified throughout the septotemporal axis according to Eq. 2:

$$N = \Sigma Q \times 1/ssf \qquad (Eq.\ 2)$$

where 1/ssf is the inverse of the section sampling fraction (10). The dentate gyrus was used as the positive control area for cell proliferation.

Soma size of Iba1-IR cells was analyzed with ImageJ software. Images underwent automated thresholding, and the areas occupied by the somas were obtained by performing the analyze particle function and expressed as square micrometers per cell. A soma size >65 μm^2 was used as an indicator of activated microglia (21).

The phenotype of BrdU-IR cells was analyzed by using a confocal microscope with HeNe and Ar lasers (Leica DM2500 TCS SPE) with a 63× objective (1.4 numerical aperture) and through the z-axis at 0.6-μm intervals.

Twenty-nine sections containing the ARC from five animals were analyzed. Within the ARC, 173 BrdU-IR cells and 1,095 Iba1-IR cells were analyzed. Sections were automatically scored for double labeling with ImageJ software.

Statistical Analysis

Values are reported as mean ± SEM. Data were analyzed by unpaired Student t test or by one-way, two-way, or two-way repeated ANOVA followed by Fisher least significant difference post hoc analysis. $P < 0.05$ denotes statistical significance.

RESULTS

HFD Specifically Induces Cell Proliferation in the ARC

Eight-week-old male chow-fed mice centrally received BrdU with or without AraC for 4 weeks. After 1 week from the surgery, animals either continued to eat chow or were switched to an HFD or a VHFD for 3 weeks (Supplementary Fig. 1A). After 4 weeks of central BrdU infusion, BrdU-IR cells were detected in the parenchyma surrounding the third ventricle and specifically in the ARC of chow-aCSF mice (Fig. 1A and B). Three weeks of HFD consumption doubled the number of BrdU-IR cells in the ARC (Fig. 1A and B), whereas it did not affect cell proliferation in the PVN, ventromedial nucleus, or dentate gyrus (Supplementary Fig. 1B–D). Conversely, feeding with a VHFD did not alter cell proliferation in the ARC (Supplementary Fig. 2A). Infusion of AraC within the lateral ventricle completely abolished (no BrdU-IR cells observed) cell proliferation in both the hypothalamus and the hippocampus, regardless of the diet.

Blockade of Cell Proliferation Blunts HFD-Induced Weight Gain by Decreasing Food Intake

Three weeks of HFD consumption increased weight, caloric intake, and fat mass while reducing lean mass gain (Fig. 1C–F). AraC treatment during HFD blunted the increase in body weight, caloric intake, and fat mass and preserved lean mass gain (Fig. 1C–F). The decrease in food intake accounted for the effect on weight because the feed efficiency was comparable between HFD-aCSF– and HFD-AraC–treated animals (Fig. 1G). Conversely, AraC had no effect in chow-fed (Fig. 1C–G) or VHFD-fed mice (Supplementary Fig. 2B–E). HFD intake altered plasma glucose, insulin, and HOMA of insulin resistance, which were not further modified by AraC (Supplementary Fig. 3).

The inhibition of hyperphagia induced by AraC in HFD-fed mice was particularly evident during the first week of HFD, when animals typically show an increase in energy intake, which wanes over time (Supplementary Fig. 4) (9,22). We analyzed changes in neuropeptides known to regulate this behavior after 1 week of HFD. AraC treatment in HFD-fed mice significantly suppressed the mRNA expression of AgRP (Fig. 2A) and tended to do so for neuropeptide Y (NPY) (Fig. 2B); both are orexigenic peptides produced in the ARC. Consistent with previous evidence (23), short exposure to HFD enhanced the hypothalamic mRNA levels of the anorectic POMC (Fig. 2C), likely in the attempt to counterregulate the caloric overload. AraC

completely prevented this effect (Fig. 2C). Expression of neuropeptides produced outside the ARC, such as the corticotrophin-releasing hormone (CRH) in the PVN or the melanin-concentrating hormone (MCH) and prepro-orexin in the lateral hypothalamus, were not altered by either the diet or the AraC treatment (Fig. 2D–F). After 1 week of HFD, cell proliferation tended to increase in the ARC (BrdU-IR cells 1,558 ± 277.8 vs. 2,779 ± 829.6/mm^3 in chow-aCSF vs. HFD-aCSF, respectively; $t_7 = 1.256$; $P = 0.25$; $n = 4$–5 mice/group). At this time, AraC had already abolished proliferation (no BrdU-IR cells observed) in the hypothalamus and hippocampus. Thus, inhibition of cell genesis affects ARC neuronal responses, which likely participate in the hyperphagia observed during HFD exposure.

Blockade of Cell Proliferation Restores Hypothalamic Leptin Sensitivity and Decreases Peripheral Inflammation

A characteristic of animals that show changes in fat mass is that fat mass changes are usually linked to changes in plasma leptin levels. After 3 weeks of HFD, plasma leptin levels were significantly reduced in HFD AraC mice compared with HFD-aCSF–treated animals, and they were undistinguishable from those observed in chow-fed mice (Fig. 3A). Conversely, consumption of a VHFD modestly increased plasma leptin levels, which were not altered by AraC (Supplementary Fig. 2F). Therefore, we evaluated changes in hypothalamic leptin-dependent signaling. AraC fully prevented the typical HFD-induced increase in the expression of SOCS3, the inhibitor of leptin signaling (Fig. 3B), while partly blunting STAT3 phosphorylation (Fig. 3C), suggesting overall the reestablishment of normal hypothalamic leptin sensitivity.

Leptin is a proinflammatory cytokine implicated in the low-grade inflammation observed in diet-induced obesity (24,25). Therefore, we assessed changes in other proinflammatory cytokines and found that AraC treatment completely prevented the HFD-dependent increase in plasma IL-1β (Fig. 4A) so that HFD-AraC and chow-aCSF mice had similar levels of this cytokine. Chow-AraC–treated animals were not included in this analysis because they were behaviorally and molecularly indistinguishable from chow-aCSF animals (Figs. 1–3). Differently from IL-1β, no change in circulating TNF-α was observed in response to either the diet or the treatment (Fig. 4B). Because macrophages are a main source of cytokines (26), we evaluated phenotypic changes of macrophages from the peritoneal cavity, a preferred site for the collection of naive tissue-resident macrophages (27). Peritoneal proinflammatory CD86-IR macrophages were reduced in HFD-AraC compared with HFD-aCSF mice (Fig. 4C), although the pool of anti-inflammatory CD36-IR macrophages was unchanged (Fig. 4D).

Blockade of Cell Proliferation Prevents Hypothalamic Neuroinflammation

Having found that AraC treatment inhibited peripheral inflammation in HFD-fed mice, we focused on hypothalamic
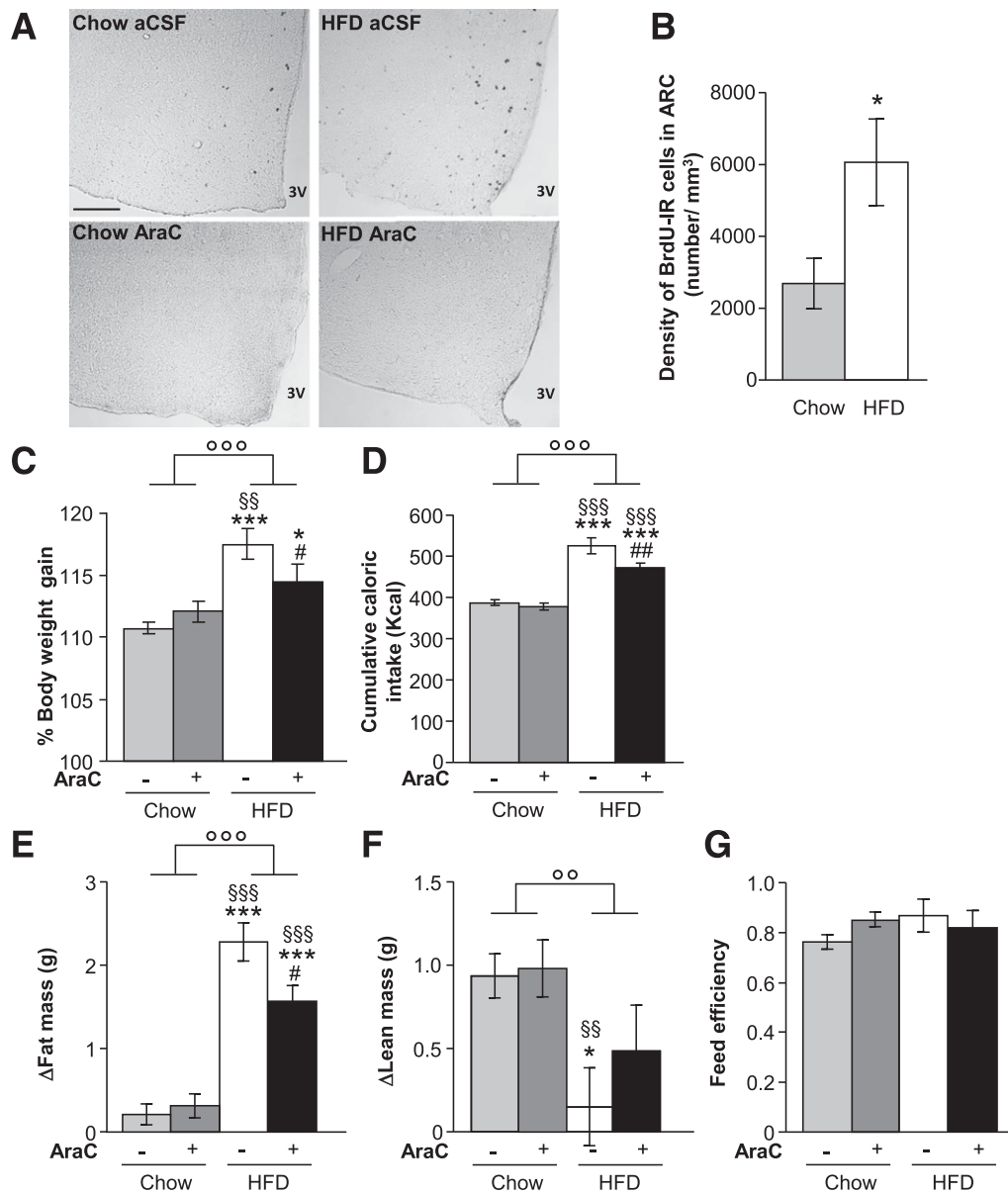
Figure 1—Inhibition of cell proliferation in the mouse adult hypothalamus hinders HFD-induced body weight gain and adiposity by decreasing caloric intake. A: Representative staining for BrdU in the ARC of chow- or HFD-fed mice treated or not with AraC. Scale bar = 15 μm. B: Density of BrdU-IR cells in the ARC (t_9 = 2.288; $P < 0.05$; n = 5–6 mice/group). C–G: Body weight gain [two-way ANOVA: diet effect $F_{(1,33)}$ = 15.46, $P < 0.0005$; treatment effect $F_{(1,33)}$ = 0.4085, $P = 0.53$; interaction $F_{(1,33)}$ = 5.077, $P < 0.05$; n = 9–10 mice/group], caloric intake [two-way ANOVA: diet effect $F_{(1,33)}$ = 68.96, $P < 0.0005$; treatment effect $F_{(1,33)}$ = 5.248, $P < 0.05$; interaction $F_{(1,33)}$ = 4.146, $P < 0.05$; n = 9–10 mice/group], difference in fat mass [two-way ANOVA: diet effect $F_{(1,33)}$ = 84.22, $P < 0.0005$; treatment effect $F_{(1,33)}$ = 2.867, $P = 0.10$; interaction $F_{(1,33)}$ = 5.041, $P < 0.05$; n = 9–10 mice/group], difference in lean mass [two-way ANOVA: diet effect $F_{(1,33)}$ = 9.111, $P < 0.005$; treatment effect $F_{(1,33)}$ = 0.799, $P = 0.377$; interaction $F_{(1,33)}$ = 0.471, $P = 0.49$; n = 9–10 mice/group], and feed efficiency [two-way ANOVA: diet effect $F_{(1,33)}$ = 0.4492, $P = 0.51$; treatment effect $F_{(1,33)}$ = 0.1421, $P = 0.71$; interaction $F_{(1,33)}$ = 1.686, $P = 0.2$; n = 9–10 mice/group] in chow- and HFD-fed mice treated or not with AraC. *$P < 0.05$, ***$P < 0.0005$ vs. chow-aCSF; §§$P < 0.005$, §§§$P < 0.0005$ vs. chow-AraC; #$P < 0.05$, ##$P < 0.005$ vs. HFD-aCSF; °°$P < 0.005$, °°°$P < 0.0005$ diet effect. 3V, third ventricle.

inflammation. HFD consumption caused microglia accumulation in the ARC (Fig. 5A and B), with the microglia, labeled with Iba1, displaying the typical morphology of activated cells with enlarged soma size (Fig. 5A–C). AraC during HFD decreased the number of Iba1-IR cells (Fig. 5A and B) and blunted the characteristic morphological changes of microglial activation (Fig. 5C). Of note, the number of ARC Iba1-IR cells

correlated with plasma leptin levels (Pearson r = 0.57; $P <$ 0.05). Microglia number or morphology was not altered in the hippocampus, suggesting that microglia activation was not generalized to the whole brain (Supplementary Fig. 5A and B). Besides, HFD-aCSF–treated mice displayed a strong expression of TNF-α in the ARC, highly colocalized with Iba1 (Fig. 5D and E). This HFD-dependent increase in TNF-α was
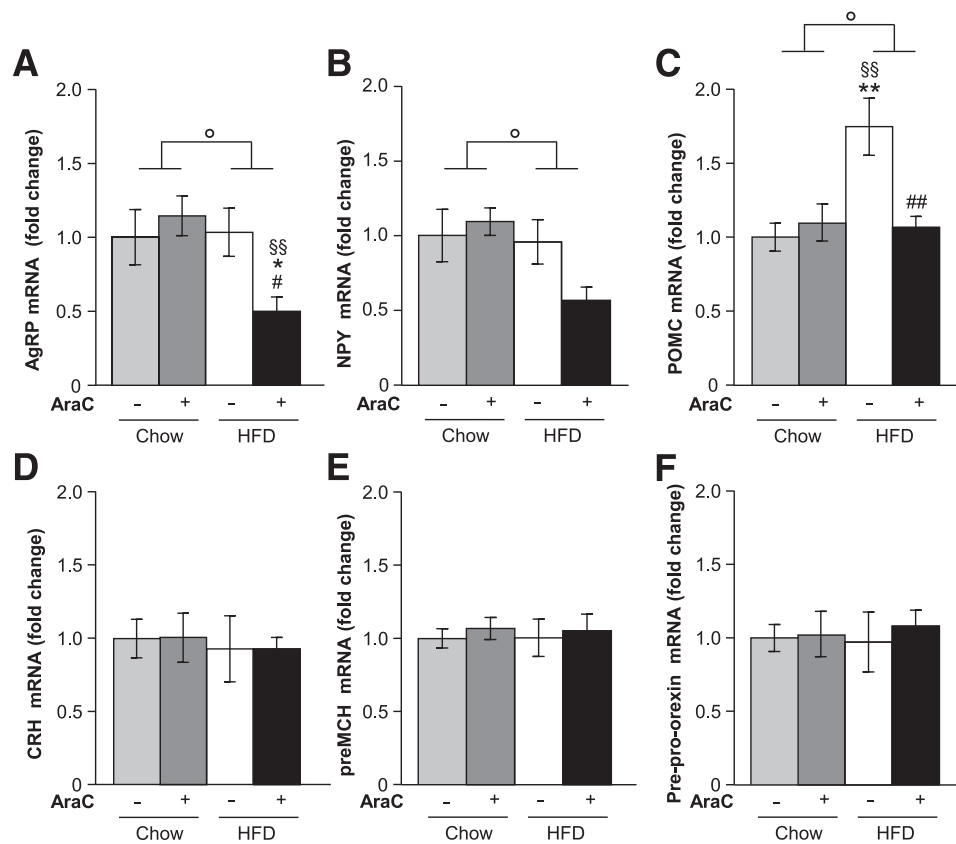
Figure 2—Blockade of cell proliferation affects hypothalamic neuropeptide expression. *A–F*: mRNA expression levels of AgRP [two-way ANOVA: diet effect $F_{(1,16)} = 4.63$, $P < 0.05$; treatment effect $F_{(1,16)} = 1.877$, $P = 0.19$; interaction $F_{(1,16)} = 5.66$, $P < 0.05$; $n = 4–6$ mice/group], NPY [two-way ANOVA: diet effect $F_{(1,16)} = 5.543$, $P < 0.05$; treatment effect $F_{(1,16)} = 1.531$, $P = 0.23$; interaction $F_{(1,16)} = 4.011$, $P = 0.062$; $n = 4–6$ mice/group], POMC [two-way ANOVA: diet effect $F_{(1,16)} = 8.15$, $P < 0.05$; treatment effect $F_{(1,16)} = 5.39$, $P < 0.05$; interaction $F_{(1,16)} = 9.75$, $P < 0.05$; $n = 4–6$ mice/group], CRH [two-way ANOVA: diet effect $F_{(1,16)} = 0.24$, $P = 0.63$; treatment effect $F_{(1,16)} = 0.001$, $P = 0.97$; interaction $F_{(1,16)} = 0.001$, $P = 0.97$; $n = 4–6$ mice/group], pre-MCH [two-way ANOVA: diet effect $F_{(1,16)} = 0.002$, $P = 0.96$; treatment effect $F_{(1,16)} = 0.32$, $P = 0.57$; interaction $F_{(1,16)} = 0.009$, $P = 0.92$; $n = 4–6$ mice/group], and prepro-orexin [two-way ANOVA: diet effect $F_{(1,16)} = 0.008$, $P = 0.92$; treatment effect $F_{(1,16)} = 0.21$, $P = 0.65$; interaction $F_{(1,16)} = 0.079$, $P = 0.78$; $n = 4–6$ mice/group] in the hypothalamus of mice maintained on chow or HFD for 1 week and treated or not with AraC. *$P < 0.05$, **$P < 0.005$ vs. chow-aCSF; §§$P < 0.005$ vs. chow-AraC; #$P < 0.05$, ##$P < 0.005$ vs. HFD-aCSF; °$P < 0.05$ diet effect.

prevented by AraC treatment (Fig. 5*D* and *E*). Accordingly, hypothalamic protein levels of IκBα, a negative regulator of NF-κB inhibited by TNF-α (28), were decreased by HFD and tended to be restored by AraC (Fig. 5*F*).

We then determined the phenotype of the newly generated cells in the ARC of HFD-fed mice. Double labeling of BrdU-IR cells with Iba1 (Fig. 6*A–C*) revealed strong colocalization (43 ± 9% of BrdU-IR cells were labeled Iba1). In contrast, BrdU-IR cells did not express GFAP (Fig. 6*A*), a marker of astrocytes, or NeuN, a marker of mature neurons (Fig. 6*A*).

Altogether, these results suggest that HFD consumption causes rapid expansion and proinflammatory activation of microglia in the ARC and that blockade of this process prevents both hypothalamic and peripheral inflammation while blunting excessive caloric intake and body weight gain.

DISCUSSION

Both central and peripheral inflammation contribute to diet-induced obesity, insulin resistance, and type 2 diabetes

(29). Consumption of an HFD causes inflammation in the hypothalamus (4,9,12,30); however, the underlying mechanisms remain poorly understood.

We demonstrate that exposure for a brief period (up to 3 weeks) to a diet rich in saturated fats induces cell genesis in the ARC. Stimulation of cell proliferation leads to new microglia with a proinflammatory phenotype, which is associated with increased caloric intake, body weight gain, and peripheral inflammation, all changes that could be prevented in part or completely by inhibiting cell proliferation through the central delivery of AraC.

HFD specifically increases cell proliferation in the ARC, but not in other hypothalamic nuclei or well-known cell proliferative and neurogenic structures, such as the dentate gyrus of the hippocampus (31). This cell proliferative response, in turn, results in microglia expansion. Microglia are known to take up residence in the CNS during development (32) and can self-renew in the adult brain (33–35). Differently from other brain areas, the
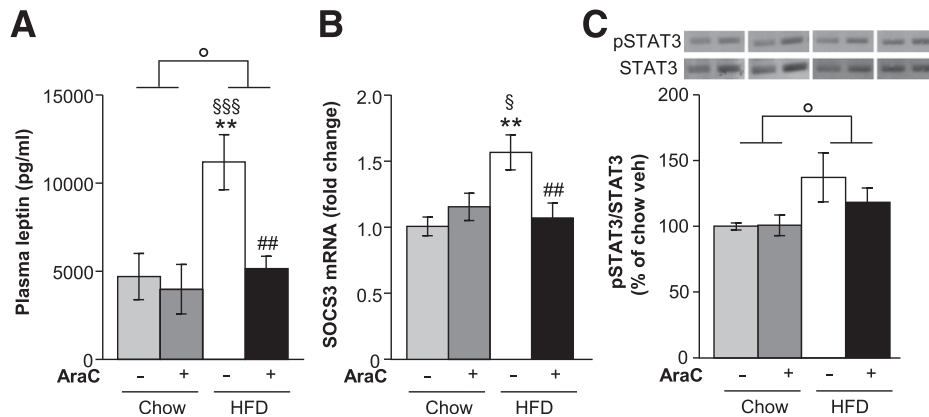
Figure 3—AraC administration restores hypothalamic sensitivity to leptin. *A*: Plasma leptin levels of chow- and HFD-fed mice treated or not with AraC [two-way ANOVA: diet effect $F_{(1,29)} = 9.19$, $P < 0.05$; treatment effect $F_{(1,29)} = 7.17$, $P < 0.05$; interaction $F_{(1,29)} = 4.46$, $P < 0.05$; $n = 8–9$ mice/group]. *B*: Hypothalamic mRNA expression levels of SOCS3 in chow- and HFD-fed mice treated or not with AraC [two-way ANOVA: diet effect $F_{(1,15)} = 4.394$, $P = 0.053$; treatment effect $F_{(1,15)} = 2.367$, $P = 0.144$; interaction $F_{(1,15)} = 8.404$, $P < 0.05$; $n = 4–6$ per group]. *C*: Representative Western blots and quantification of p-STAT3 [two-way ANOVA: diet effect $F_{(1,15)} = 5.421$, $P < 0.05$; treatment effect $F_{(1,15)} = 0.588$, $P = 0.455$; interaction $F_{(1,15)} = 0.691$, $P = 0.419$; $n = 4–5$ mice/group] protein expression in the mediobasal hypothalamus of chow- and HFD-fed mice treated or not with AraC. **$P < 0.005$ vs. chow-aCSF; §$P < 0.05$, §§§$P < 0.0005$ vs. chow-AraC; ##$P < 0.005$ vs. HFD-aCSF; °$P < 0.05$ diet effect. veh, vehicle.

ARC is vascularized by fenestrated vessels that facilitate the passage of circulating signaling molecules (36). This anatomical characteristic probably explains why inflammatory responses are readily observed in this brain area compared with other brain structures. This explanation also holds true for obese humans, where exacerbated microglia dystrophy is observed in the mediobasal hypothalamus but not in the cortex or amygdala (9,37). Evidence suggests that microglia work in the ARC as a sensor of saturated fatty acids (38). Such function is particularly
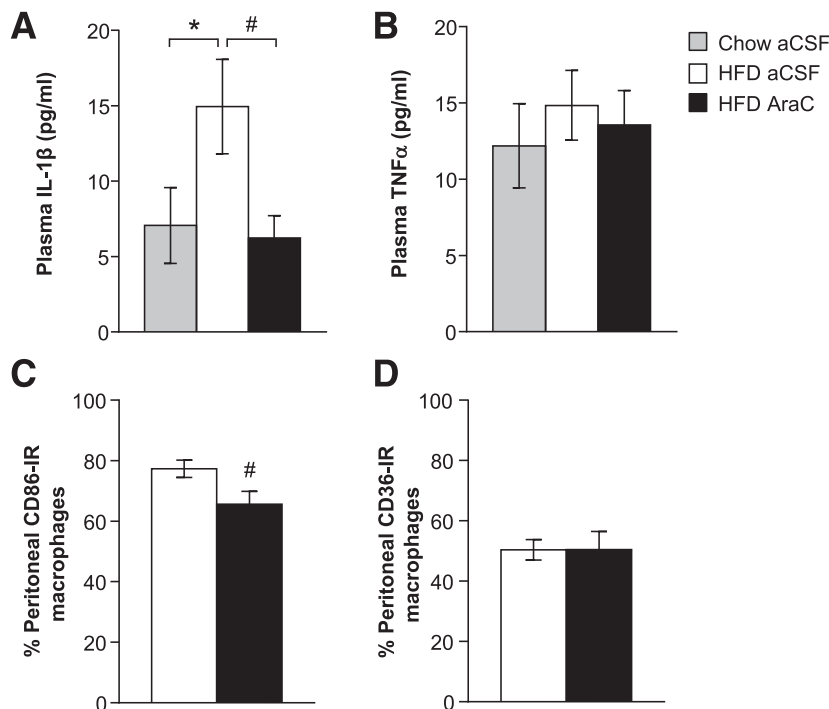

Figure 4—AraC administration inhibits HFD-induced peripheral inflammation. *A* and *B*: Plasma IL-1β [one-way ANOVA: $F_{(2,23)} = 3.659$, $P < 0.05$; $n = 8–9$ mice/group] and plasma TNFα [one-way ANOVA: $F_{(2,24)} = 0.2977$, $P = 0.75$; $n = 8–10$ mice/group] levels in chow-aCSF–, HFD-aCSF–, and HFD-AraC–treated mice. *C* and *D*: FACS analysis of peritoneal proinflammatory CD86-IR ($t_{10} = 2.301$, $P < 0.05$; $n = 6$ mice/group) and anti-inflammatory CD36-IR ($t_{10} = 0.007$, $P = 0.9$; $n = 6$ mice/group) macrophages from HFD-fed mice treated or not with AraC. *$P < 0.05$ vs. chow-aCSF; #$P < 0.05$ vs. HFD-aCSF.
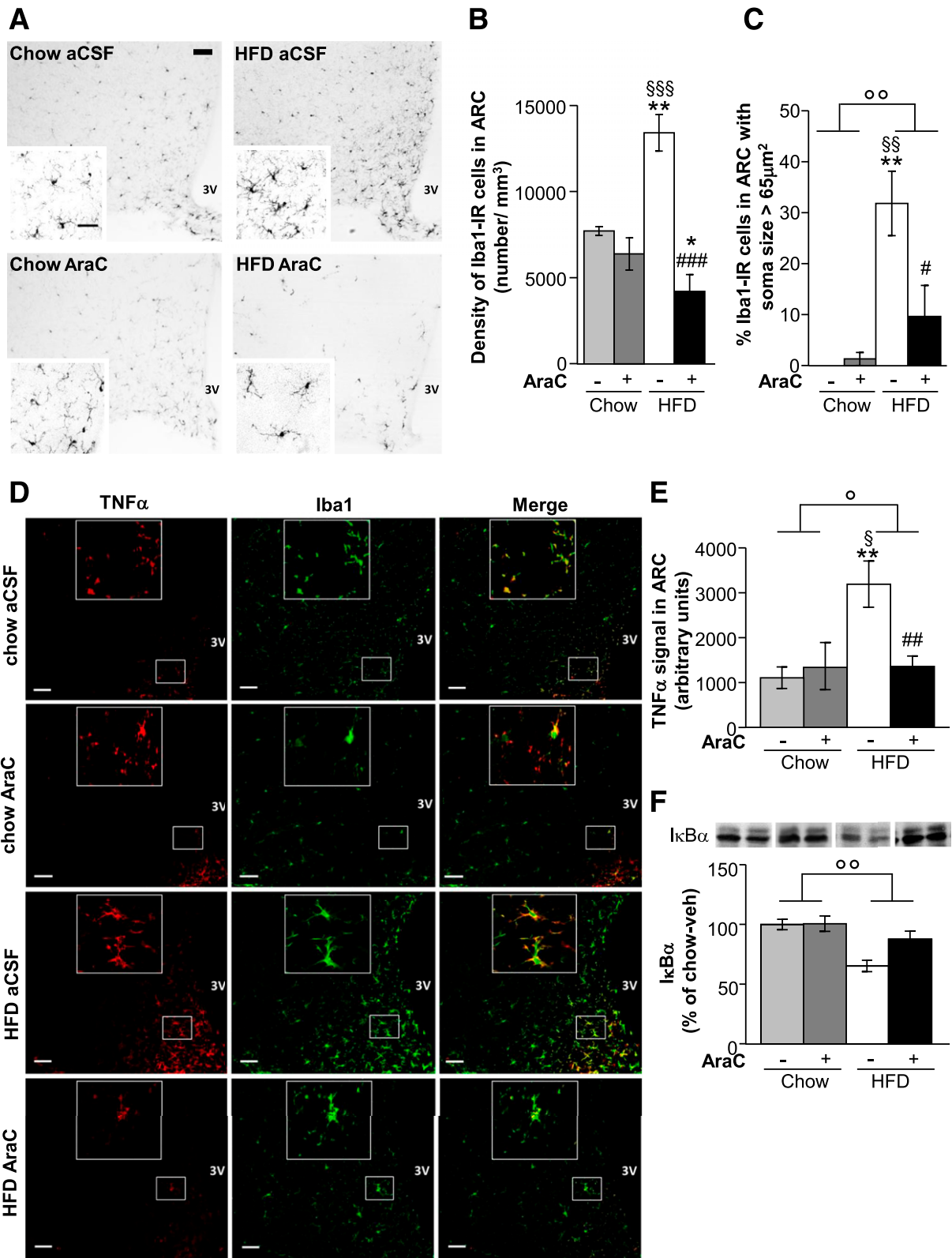
Figure 5—HFD-induced hypothalamic inflammation is blocked by AraC. *A*: Representative images and higher magnification inset of microglial cells labeled with Iba1 in the ARC of chow- and HFD-fed mice treated or not with AraC. Scale bar = 15 μm (main panel) and 4 μm (inset). *B*: Quantification of Iba1 staining in the ARC [two-way ANOVA: diet effect $F_{(1,13)}$ = 3.162, *P* = 0.09; treatment effect $F_{(1,13)}$ = 28.19, *P* < 0.0005; interaction $F_{(1,13)}$ = 15.73, *P* < 0.005; *n* = 3–5 mice/group]. *C*: Percentage of Iba1-IR cells in the ARC with soma size >65 μm^2 [two-way ANOVA: diet effect $F_{(1,13)}$ = 13.75, *P* < 0.005; treatment effect $F_{(1,13)}$ = 3.701, *P* = 0.076; interaction $F_{(1,13)}$ = 4.674, *P* < 0.05; *n* = 3–5 mice/group]. *D*: Representative confocal pictures of the double staining against TNF-α (red) and Iba1 (green) in the ARC of chow- and HFD-fed mice treated or not with AraC. Scale bars = 25 μm. *E*: Quantification of TNF-α staining in the ARC [two-way ANOVA:

fitting, considering the ability of ARC neurons to rapidly sense and integrate nutrient changes to modify behavior (10). Consequently, different nutrient-related signals would be expected to differentially affect cell proliferation in the ARC. This conclusion is supported by our observation that microglia expansion in the ARC depends on the type of diet consumed. Indeed, when animals ate a VHFD with a content of saturated fats comparable to that of the HFD but with only 5% of calories from carbohydrates, which are abundant in chow, cell proliferation was indistinguishable from that observed in chow-fed mice. Consumption of saturated fat, therefore, likely increases cell proliferation only when associated with appropriate intake (>5%) of carbohydrates. Besides, inhibition of cell proliferation in chow did not alter energy balance or inflammatory responses, implying that this process becomes relevant only when engaged as a counterregulatory mechanism in response to physiologic or environmental changes (39).

The type of diet used and the relatively short exposure to it could explain why we observed proliferation of microglia but not of neurons or astrocytes in the ARC. This point is critical because of conflicting evidence about the role and nature of hypothalamic cell proliferation. In fact, some studies have shown that inhibition of hypothalamic cell proliferation decreases body weight (39–41), which agrees with the current findings, whereas others describe an increase in body weight (42,43). In particular, neurogenesis has been found in the ARC (44,45). However, HFD feeding can suppress neurogenesis (41,46), not alter the neuronal fate rate (43), or induce (~6% increase) the generation of new neurons in this area in a sex- and age-dependent manner (40,41). Moreover, astrogliosis is present in the ARC of obese animals and humans (9,13,37) but could be a consequence of signals from activated microglia.

Several technical factors such as the route and length of BrdU administration, the time point of the neuroanatomical analysis, and the age and sex of the animals studied could help to explain these seemingly contradictory findings. Besides, although BrdU labels all proliferating cells, some of these cells are immature or dying (47).

The current data demonstrate that cell proliferation is required to observe the HFD-associated inflammatory response in the ARC because AraC treatment in HFD-fed mice prevented the increase in hypothalamic microglia activation and blunted the recruitment of the NF-κB pathway. Of note, HFD consumption does not alter microglia functionality because microglia from HFD-fed animals retain full ability to respond to additional stimuli (i.e., lipopolysaccharide) and react to changes in their surroundings (7,37). However, microglia activation not only is the result of the action of specific saturated fatty acids introduced with the diet but also can be linked to other nutrient (i.e., related to high-sucrose intake) and hormonal signals, for which changes in circulating levels are observed in conditions other than HFD consumption (7,16,38,48,49). In particular, increased levels of circulating leptin and cytokines induce microglia activation (16,50–54). We observed augmented plasma leptin and IL-1β levels in HFD-fed mice, which might have activated existing microglia in the ARC. In support of this interpretation, a positive correlation was found between plasma leptin and number of ARC Iba1-IR cells. As for IL-1β, its release from microglia can be stimulated by leptin (52), and hypothalamic increase in IL-1β signaling due to early overnutrition is associated with defective melanocortin signaling, which favors food intake (55).

The current results differ from those of previous studies where HFD-induced hypothalamic inflammation was observed in the absence of peripheral inflammation (7,9). This difference may rely on the techniques used and signals investigated because we studied circulating levels of cytokines by immunoassay and looked at peritoneal macrophage phenotypes by FACS, whereas others have performed quantitative real-time PCR for inflammatory markers in peripheral tissues (7,9). Alternatively, diet might have a direct effect on peripheral immune cells because monocytes have nutrient-related receptors of which expression correlates with a range of metabolic and inflammatory markers (56,57).

Further studies will clarify whether the decreased peripheral inflammation induced by AraC is due to the decrease in fat mass observed or whether other mechanisms that directly link central with peripheral inflammatory responses might instead be involved. The latter hypothesis is supported by the observation that although AraC treatment only partly inhibits fat mass gain in HFD-fed mice, it completely prevents increases in plasma leptin and IL-1β levels.

Blockade of cell proliferation during HFD exposure may also alter microglia-neuron interaction. The typical increase in caloric intake during the first week of HFD (9,22) is blunted by AraC treatment. This reduction in caloric intake is associated with changes in the expression of neuropeptides produced by ARC neurons. Thaler et al. (9) found that feeding rats an HFD (the same one we used) for 1 week increased Iba1 staining and caused

---

diet effect $F_{(1,17)} = 7.098$, $P < 0.05$; treatment effect $F_{(1,17)} = 3.99$, $P = 0.062$; interaction $F_{(1,17)} = 7.624$, $P < 0.05$; $n = 4–7$ mice/group]. F: IκBα protein expression in the mediobasal hypothalamus of chow- and HFD-fed mice treated or not with AraC [two-way ANOVA: diet effect $F_{(1,15)} = 18.58$, $P < 0.005$; treatment effect $F_{(1,15)} = 4.389$, $P = 0.053$; interaction $F_{(1,15)} = 3.911$, $P = 0.066$; $n = 4–5$ mice/group]. *$P < 0.05$, **$P < 0.005$ vs. chow-aCSF; §$P < 0.05$, §§$P < 0.005$, §§§$P < 0.0005$ vs. chow-AraC; #$P < 0.05$, ##$P < 0.005$, ###$P < 0.0005$ vs. HFD-aCSF; °$P < 0.05$, °°$P < 0.005$ diet effect. 3V, third ventricle; veh, vehicle.
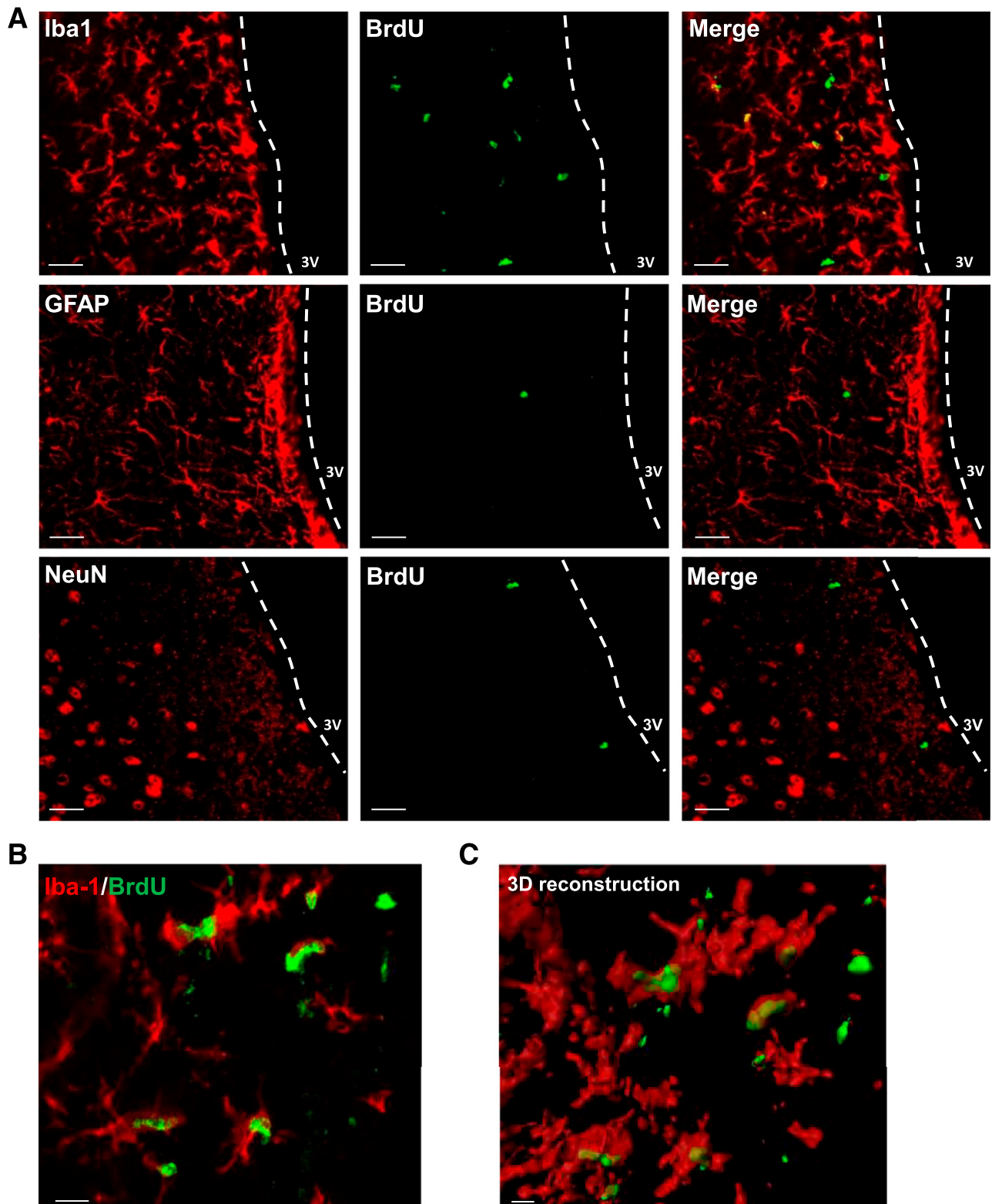
Figure 6—HFD feeding leads to hypothalamic microglia proliferation. *A*: Representative confocal images of coimmunodetection of BrdU (green) with Iba1, GFAP, or NeuN (red). Scale bars = 20 μm. *B* and *C*: Representative higher magnification and three-dimensional reconstruction of the colocalized Iba1/BrdU (red/green) staining. Scale bars = 7 μm (*B*) and 5 μm (*C*). 3V, third ventricle.

neuronal stress as assessed by the increased expression of the chaperon protein Hsp72 in ARC neurons. Valdearcos et al. (38) described similar results after 4 weeks of HFD or even short-term (3 days) administration of saturated fatty acids by gavage. In the latter study, microglia depletion abolished Hsp72 expression in neurons, suggesting

that neuronal stress is triggered by increased microglia activity. Neuronal stress in response to HFD is associated with increased NF-κB signaling (12). Conversely, genetic deletion of Iκβ kinase subunit β (a component of the NF-κB pathway) in AgRP neurons decreases HFD intake (12). In the current study, HFD-fed mice had increased hypothalamic expression of SOCS3, which is a marker of augmented NF-κB activity (12), and decreased IκBα protein, a negative regulator of NF-κB (58). These changes were prevented by AraC. Thus, blockade of cell genesis, by reducing microglia proliferation and activity, probably blunts neuronal stress responses, resulting in changes in neuropeptides known to affect feeding.

Altogether, the evidence we provide linking consumption of a high saturated fat diet with hypothalamic proinflammatory microglia proliferation and body weight gain underscores the physiological relevance of our findings to humans, many of whom consume diets rich in carbohydrates and saturated fats.

References

1. Calder PC, Ahluwalia N, Brouns F, et al. Dietary factors and low-grade inflammation in relation to overweight and obesity. Br J Nutr 2011;106(Suppl. 3):S5–S78

2. Dalmas E, Clément K, Guerre-Millo M. Defining macrophage phenotype and function in adipose tissue. Trends Immunol 2011;32:307–314

3. Brestoff JR, Artis D. Immune regulation of metabolic homeostasis in health and disease. Cell 2015;161:146–160

4. De Souza CT, Araujo EP, Bordin S, et al. Consumption of a fat-rich diet activates a proinflammatory response and induces insulin resistance in the hypothalamus. Endocrinology 2005;146:4192–4199

5. Dinel AL, André C, Aubert A, Ferreira G, Layé S, Castanon N. Cognitive and emotional alterations are related to hippocampal inflammation in a mouse model of metabolic syndrome. PLoS One 2011;6:e24325

6. Boitard C, Cavaroc A, Sauvant J, et al. Impairment of hippocampal-dependent memory induced by juvenile high-fat diet intake is associated with enhanced hippocampal inflammation in rats. Brain Behav Immun 2014;40:9–17

7. Maric T, Woodside B, Luheshi GN. The effects of dietary saturated fat on basal hypothalamic neuroinflammation in rats. Brain Behav Immun 2014;36:35–45

8. André C, Dinel AL, Ferreira G, Layé S, Castanon N. Diet-induced obesity progressively alters cognition, anxiety-like behavior and lipopolysaccharide-induced depressive-like behavior: focus on brain indoleamine 2,3-dioxygenase activation. Brain Behav Immun 2014;41:10–21

9. Thaler JP, Yi CX, Schur EA, et al. Obesity is associated with hypothalamic injury in rodents and humans. J Clin Invest 2012;122:153–162

10. Cota D, Proulx K, Seeley RJ. The role of CNS fuel sensing in energy and glucose regulation. Gastroenterology 2007;132:2158–2168

11. Sohn JW, Elmquist JK, Williams KW. Neuronal circuits that regulate feeding behavior and metabolism. Trends Neurosci 2013;36:504–512

12. Zhang X, Zhang G, Zhang H, Karin M, Bai H, Cai D. Hypothalamic IKKbeta/NF-kappaB and ER stress link overnutrition to energy imbalance and obesity. Cell 2008;135:61–73

13. Horvath TL, Sarman B, García-Cáceres C, et al. Synaptic input organization of the melanocortin system predicts diet-induced hypothalamic reactive gliosis and obesity. Proc Natl Acad Sci U S A 2010;107:14875–14880

14. Milanski M, Arruda AP, Coope A, et al. Inhibition of hypothalamic inflammation reverses diet-induced insulin resistance in the liver. Diabetes 2012;61:1455–1462

15. Ozcan L, Ergin AS, Lu A, et al. Endoplasmic reticulum stress plays a central role in development of leptin resistance. Cell Metab 2009;9:35–51

16. Gao Y, Ottaway N, Schriever SC, et al. Hormones and diet, but not body weight, control hypothalamic microglial activity. Glia 2014;62:17–25

17. Sousa-Ferreira L, de Almeida LP, Cavadas C. Role of hypothalamic neurogenesis in feeding regulation. Trends Endocrinol Metab 2014;25:80–88

18. Binder E, Bermúdez-Silva FJ, André C, et al. Leucine supplementation protects from insulin resistance by regulating adiposity levels. PLoS One 2013;8:e74705

19. Cardinal P, André C, Quarta C, et al. CB1 cannabinoid receptor in SF1-expressing neurons of the ventromedial hypothalamus determines metabolic responses to diet and leptin. Mol Metab 2014;3:705–716

20. Dinel AL, André C, Aubert A, Ferreira G, Layé S, Castanon N. Lipopolysaccharide-induced brain activation of the indoleamine 2,3-dioxygenase and depressive-like behavior are impaired in a mouse model of metabolic syndrome. Psychoneuroendocrinology 2014;40:48–59

21. Kozlowski C, Weimer RM. An automated method to quantify microglia morphology and application to monitor activation state longitudinally in vivo. PLoS One 2012;7:e31814

22. Benani A, Hryhorczuk C, Gouazé A, et al. Food intake adaptation to dietary fat involves PSA-dependent rewiring of the arcuate melanocortin system in mice. J Neurosci 2012;32:11970–11979

23. Ziotopoulou M, Mantzoros CS, Hileman SM, Flier JS. Differential expression of hypothalamic neuropeptides in the early phase of diet-induced obesity in mice. Am J Physiol Endocrinol Metab 2000;279:E838–E845

24. Matarese G, Procaccini C, De Rosa V, Horvath TL, La Cava A. Regulatory T cells in obesity: the leptin connection. Trends Mol Med 2010;16:247–256

25. Aguilar-Valles A, Inoue W, Rummel C, Luheshi GN. Obesity, adipokines and neuroinflammation. Neuropharmacology 2015;96(Pt A):124–134

26. Chawla A, Nguyen KD, Goh YP. Macrophage-mediated inflammation in metabolic disease. Nat Rev Immunol 2011;11:738–749

27. Zhang X, Goncalves R, Mosser DM. The isolation and characterization of murine macrophages. Curr Protoc Immunol 2008;Chapter 14:Unit 14.1

28. DiDonato JA, Hayakawa M, Rothwarf DM, Zandi E, Karin M. A cytokine-responsive IkappaB kinase that activates the transcription factor NF-kappaB. Nature 1997;388:548–554

29. Donath MY, Shoelson SE. Type 2 diabetes as an inflammatory disease. Nat Rev Immunol 2011;11:98–107

30. Milanski M, Degasperi G, Coope A, et al. Saturated fatty acids produce an inflammatory response predominantly through the activation of TLR4 signaling in hypothalamus: implications for the pathogenesis of obesity. J Neurosci 2009;29:359–370

31. Abrous DN, Koehl M, Le Moal M. Adult neurogenesis: from precursors to network and physiology. Physiol Rev 2005;85:523–569

32. Ginhoux F, Greter M, Leboeuf M, et al. Fate mapping analysis reveals that adult microglia derive from primitive macrophages. Science 2010;330:841–845

33. Ajami B, Bennett JL, Krieger C, Tetzlaff W, Rossi FM. Local self-renewal can sustain CNS microglia maintenance and function throughout adult life. Nat Neurosci 2007;10:1538–1543

34. Ajami B, Bennett JL, Krieger C, McNagny KM, Rossi FM. Infiltrating monocytes trigger EAE progression, but do not contribute to the resident microglia pool. Nat Neurosci 2011;14:1142–1149

35. Bruttger J, Karram K, Wörtge S, et al. Genetic cell ablation reveals clusters of local self-renewing microglia in the mammalian central nervous system. Immunity 2015;43:92–106

36. Ciofi P, Garret M, Lapirot O, et al. Brain-endocrine interactions: a microvascular route in the mediobasal hypothalamus. Endocrinology 2009;150:5509–5519

37. Baufeld C, Osterloh A, Prokop S, Miller KR, Heppner FL. High-fat diet-induced brain region-specific phenotypic spectrum of CNS resident microglia. Acta Neuropathol 2016;132:361–375

38. Valdearcos M, Robblee MM, Benjamin DI, Nomura DK, Xu AW, Koliwad SK. Microglia dictate the impact of saturated fat consumption on hypothalamic inflammation and neuronal function. Cell Reports 2014;9:2124–2138

39. Pierce AA, Xu AW. De novo neurogenesis in adult hypothalamus as a compensatory mechanism to regulate energy balance. J Neurosci 2010;30:723–730

40. Lee DA, Bedont JL, Pak T, et al. Tanycytes of the hypothalamic median eminence form a diet-responsive neurogenic niche. Nat Neurosci 2012;15:700–702

41. Lee DA, Yoo S, Pak T, et al. Dietary and sex-specific factors regulate hypothalamic neurogenesis in young adult mice. Front Neurosci 2014;8:157

42. Li J, Tang Y, Purkayastha S, Yan J, Cai D. Control of obesity and glucose intolerance via building neural stem cells in the hypothalamus. Mol Metab 2014;3:313–324

43. Gouazé A, Brenachot X, Rigault C, et al. Cerebral cell renewal in adult mice controls the onset of obesity. PLoS One 2013;8:e72029

44. Kokoeva MV, Yin H, Flier JS. Neurogenesis in the hypothalamus of adult mice: potential role in energy balance. Science 2005;310:679–683

45. Kokoeva MV, Yin H, Flier JS. Evidence for constitutive neural cell proliferation in the adult murine hypothalamus. J Comp Neurol 2007;505:209–220

46. McNay DE, Briançon N, Kokoeva MV, Maratos-Flier E, Flier JS. Remodeling of the arcuate nucleus energy-balance circuit is inhibited in obese mice. J Clin Invest 2012;122:142–152

47. Duque A, Rakic P. Different effects of bromodeoxyuridine and [^{3}H]thymidine incorporation into DNA on cell proliferation, position, and fate. J Neurosci 2011;31:15205–15217

48. Fuente-Martín E, García-Cáceres C, Díaz F, et al. Hypothalamic inflammation without astrogliosis in response to high sucrose intake is modulated by neonatal nutrition in male rats. Endocrinology 2013;154:2318–2330

49. Tapia-González S, García-Segura LM, Tena-Sempere M, et al. Activation of microglia in specific hypothalamic nuclei and the cerebellum of adult rats exposed to neonatal overnutrition. J Neuroendocrinol 2011;23:365–370

50. Layé S, Liège S, Li KS, Moze E, Neveu PJ. Physiological significance of the interleukin 1 receptor accessory protein. Neuroimmunomodulation 2001;9:225–230

51. Madore C, Joffre C, Delpech JC, et al. Early morphofunctional plasticity of microglia in response to acute lipopolysaccharide. Brain Behav Immun 2013;34:151–158

52. Pinteaux E, Inoue W, Schmidt L, Molina-Holgado F, Rothwell NJ, Luheshi GN. Leptin induces interleukin-1beta release from rat microglial cells through a caspase 1 independent mechanism. J Neurochem 2007;102:826–833

53. Rummel C, Inoue W, Sachot C, Poole S, Hübschle T, Luheshi GN. Selective contribution of interleukin-6 and leptin to brain inflammatory signals induced by systemic LPS injection in mice. J Comp Neurol 2008;511:373–395

54. Tang CH, Lu DY, Yang RS, et al. Leptin-induced IL-6 production is mediated by leptin receptor, insulin receptor substrate-1, phosphatidylinositol 3-kinase, Akt, NF-kappaB, and p300 pathway in microglia. J Immunol 2007;179:1292–1302

55. Grayson BE, Levasseur PR, Williams SM, Smith MS, Marks DL, Grove KL. Changes in melanocortin expression and inflammatory pathways in fetal offspring of nonhuman primates fed a high-fat diet. Endocrinology 2010;151:1622–1632

56. Martínez-Micaelo N, González-Abuín N, Terra X, et al. Identification of a nutrient-sensing transcriptional network in monocytes by using inbred rat models on a cafeteria diet. Dis Model Mech 2016;9:1231–1239

57. Pivovarova O, Hornemann S, Weimer S, et al. Regulation of nutrition-associated receptors in blood monocytes of normal weight and obese humans. Peptides 2015;65:12–19

58. Hayden MS, Ghosh S. Shared principles in NF-kappaB signaling. Cell 2008;132:344–362